remote sensing

MDPI

Project

Analysis and application of the methodology proposed in the article "U-Net for Taiwan Shoreline Detection from SAR Images" in the region of Ria Formosa, Algarve.

Sílvia Mourão [1*]

[1] Faculdade de Ciências da Universidade de Lisboa; silamourao@gmail.com;
* Correspondence: silamourao@gmail.com;

Abstract: Climate change is a serious global threat that is leading to changes in sea levels which brings an aggravated risk to coastal populations and natural areas. In order to monitor the changes occurring in shorelines, this project uses the methodology proposed in the article "U-Net for Taiwan Shoreline Detection from SAR Images" and applies it to the vulnerable region of Ria Formosa in Portugal. This methodology involves the development and training of a U-Net deep learning algorithm, which is used to perform a land-sea segmentation of the original SAR images, which is then processed to allow for an easier extraction of the shoreline with edge detection. The results obtained in this process were below the results obtained in the original work, achieving only a F1-Score of 54% with 5 pixels of difference between the detected shoreline and the ground truth data.

Keywords: Microwave remote sensing, Sentinel-1, shoreline detection, U-Net, image segmentation, shoreline change

Citation: Mourão, S., Analysis and application of the methodology proposed in the article "U-Net for Taiwan Shoreline Detection from SAR Images" in the region of Ria Formosa, Algarve. *Remote Sens.* **2022**, *14*, x. https://doi.org/10.3390/xxxxx

Received: 14/12/2022

Publisher's Note: MDPI stays neutral with regard to jurisdictional claims in published maps and institutional affiliations.

1. Introduction

Climate change is already causing large alterations to the world as we know it and it will continue to cause alterations to landscapes, shorelines, ecosystems and populations. r the last few decades there has been an increase in extreme climate phenomena, associated with the continuous rise of the Earth's average temperature. This is leading to a constant increase in the Ocean's dynamic such as thermal expansion and water mass increase, which is resulting in an accelerated rise in the sea level, causing a severe risk for coastal regions[1, 2].

Several studies show that the rate of sea level rise is increasing[3–5], which means that the potential of shoreline change and thus the erosion of coastal areas is greatly amplified[6]. Due to the imminent danger this represents to coastal populations and ecosystems it is necessary to have systems in place which can be used to monitor the sea level. The task of monitoring and managing coastal areas is of considerable social and economic importance[7].

This project was developed as a practical component for the Microwave Remote Sensing curriculum unit and its main purpose is to analyse and replicate the methodology applied by the authors in the article "U-Net for Taiwan Shoreline Detection from SAR Images"[7]. Considering the importance of continuous monitoring of sea level rise and its impact to society, the authors of this paper propose a method for detecting shoreline changes based on the use of a deep learning algorithm known as U-Net as a method for the segmentation of SAR images, followed by a process of digital image processing to

extract the boundary between land and sea, which can then be incorporated in a time series to evaluate any potential coastline changes.

The traditional methods of coastline detection are ground surveys and visual interpretation, which are accurate and detailed. However, they are also laborious and time-consuming, and thus difficult to conduct in a large area. Using remote sensing provides geospatial engineers an alternative which is less work and time intensive. There are two types of remote sensing data that can be utilized for shoreline detection, namely radar images and optical images. In general, optical images provide more detailed information for detecting the changes in a shoreline, however, the tide conditions and weather have greatly limited their applications. Therefore, the synthetic aperture radar (SAR) images have become the preferred data source for shoreline detection due to a strong penetration ability, all-day observation, high resolution, and wide spatial coverage capabilities [8, 9]

There are many studies where authors have applied various methods to extract shorelines from SAR images. Initially most of these studies used variations of differential operators for edge detection, such as edge tracing algorithms[10] or statistical active contour[11], which then evolved into semi-automatic[12] and unsupervised[13] methods. With the development of more advanced machine learning capabilities, studies started to apply algorithms such as K-means[14], fuzzy clustering [15] or super pixel segmentation [16]. In the past few years, deep learning methods have successfully reduced the computing time and achieved outstanding accuracy, even for the complex remote sensing imagery[7].

The U-net is a deep learning architecture originally utilised for segmentation of biomedical imagery[17], which has since been modified for the purpose of land-sea segmentation tasks such as the automatic detection of the Antarctic shoreline from Sentinel-1 data[18]. Several other authors have then built upon the U-Net segmentation by introducing hybrid deep learning models[19], deeper U-Net architectures (DeepUNet)[20] or constructing new U-Net structures [21, 22]. In the aforementioned studies, there was no compact formulation to evaluate the efficiency of each method due to the varied landform of the selected study areas. To bridge these gaps, the authors have collected and labelled four different types of coastal landform in order to build a shoreline dataset based on their study area in Taiwan, to which the U-Net model and edge detection methods were then applied. Finally, the authors used an image timeseries spanning six years to detect shoreline changes from the average shoreline obtained for each year in the study.

In this project the U-Net deep learning segmentation will be applied to a different study region in Portugal, an area that is also coastal and very vulnerable to climate change, and the shoreline will be extracted for three different epochs in order to try and evaluate if there has been any significant change over that time period.

2. Materials and Methods

2.1 Study Area

The study area chosen for this project is the Ria Formosa, located in the southernmost region of Portugal, Algarve, and whose boundaries can be seen in figure 1.

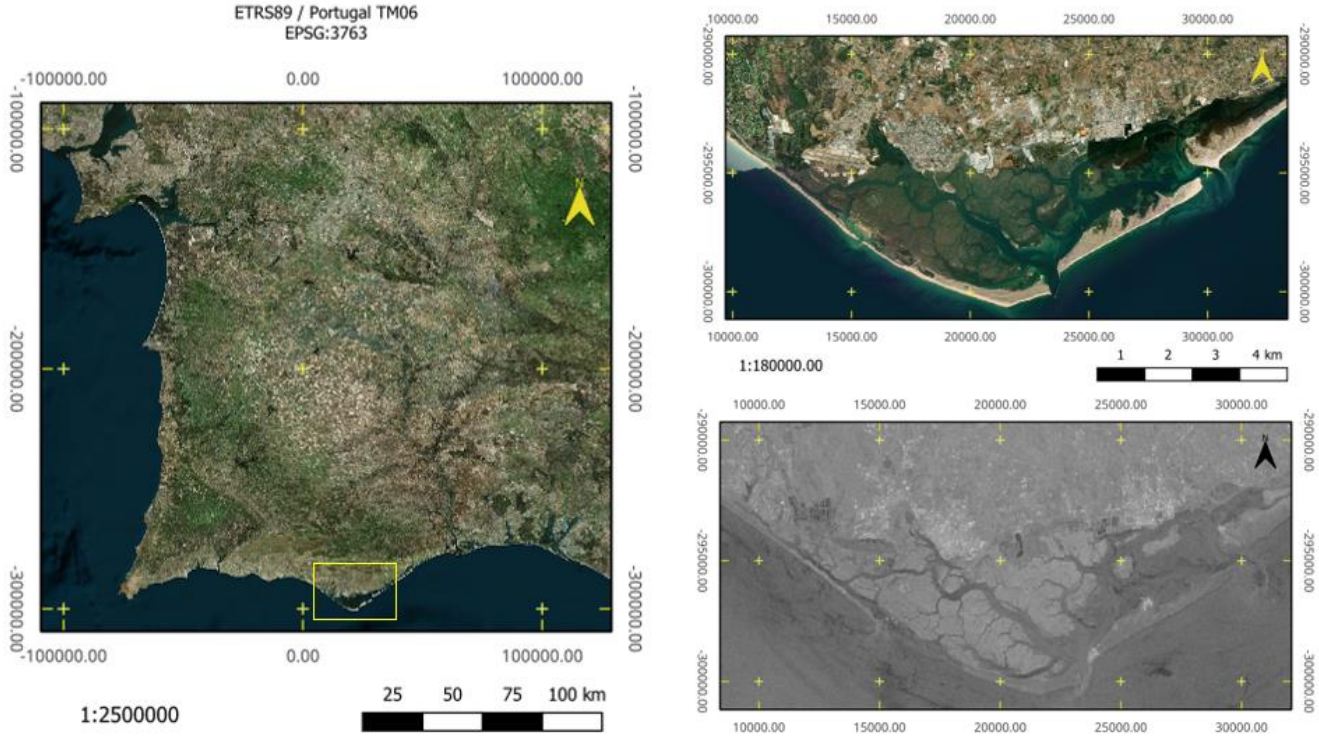

Figure 11 *- Study Area - Ria Formosa*

The Ria Formosa is a barrier lagoon that exhibits an extremely complex geometry, with innumerable channels and straits and several inlets. It includes a large intertidal zone, about 55 km long (E–W), and about 6 km (N–S) at its widest point. This is separated from the sea by two peninsular sand spits, as well as a string of barrier islands. There are seven inlets, two of which have been artificially consolidated, that allow exchanges of water with the Atlantic Ocean. A further artificial inlet was made in the west of the lagoon in 1997 [23]. The importance of the existence and persistence of tidal inlets in coastal systems is fundamental for water quality, navigability, and beach/barrier stability. The Ria Formosa is protected by a statute of Natural Reserve and constitutes a valuable regional resource for tourism, fishing, aquaculture and salt extraction industries, as well as a natural habitat for various species of birds[24]. The urban development around the lagoon places increasing pressure on this sensitive system and adds an additional layer of concern when it comes to the adaptability of the system and the impact of the rising sea level.

2.2 Image Segmentation with Otsu's Threshold

In image segmentation, thresholding is an effective tool to separate the object from the background when the grey levels are substantially different between them[25]. Otsu's Threshold method is used to perform an automatic segmentation of a grayscale image into two classes using an optimised statistical analysis[26]. The optimal value that separates the two classes results from finding the minimum value of the sum of the weighted variances for each possible threshold in the image histogram[27, 28], as described on equation 1.

$$\sigma_i^2 = w_e(t_i) \times \sigma_e^2(t_i) + w_d(t_i) \times \sigma_d^2(t_i) \quad (1)$$

However, there are limitations to the application of Otsu's method for the separation of land and sea in satellite images. One of the properties of this method is that it will bias in favour of the class with the larger variance when the within-class variance of two classes are substantially different[25]. Consequently, the application of this thresholding

technique is only valid for images where both classes are represented in a significant part of the image, which will be a conditioning factor when the images for training the network are selected.

2.3 U-Net

Deep learning is a process through which a group of machine learning algorithms attempt to model abstractions of data through a deep architecture composed of non-linear transformations. Among the several deep learning techniques, convolutional neural networks (CNNs) have been particularly popular for the purpose of classification with satellite imagery[29].

A U-Net is an architecture for semantic segmentation. It is a deep learning network which consists of a contracting path and an expansive path. The contracting path usually follows the typical architecture of a convolutional neural network, consisting in the application of two 3x3 convolutions, followed by a rectified linear unit (ReLU activation function) and a 2x2 max pooling operation. After each level is completed, there is a down sampling step, where the image size is halved. Each step on the expansive path consists of an up sampling of the image where a 2x2 convolution that undoes the down sampling step, followed by two 3x3 convolutions and a ReLU [17]. The first proposed U-Net was used for biomedical segmentation and used 23 convolutional layers [17]. Although there are many different U-Net implementations [7, 18–22] most still follow this composition and number of layers, which is also the case for the U-Net used in this project, an example of which can be seen in figure 2. It gets its name from the U shape in which its layers are organised.

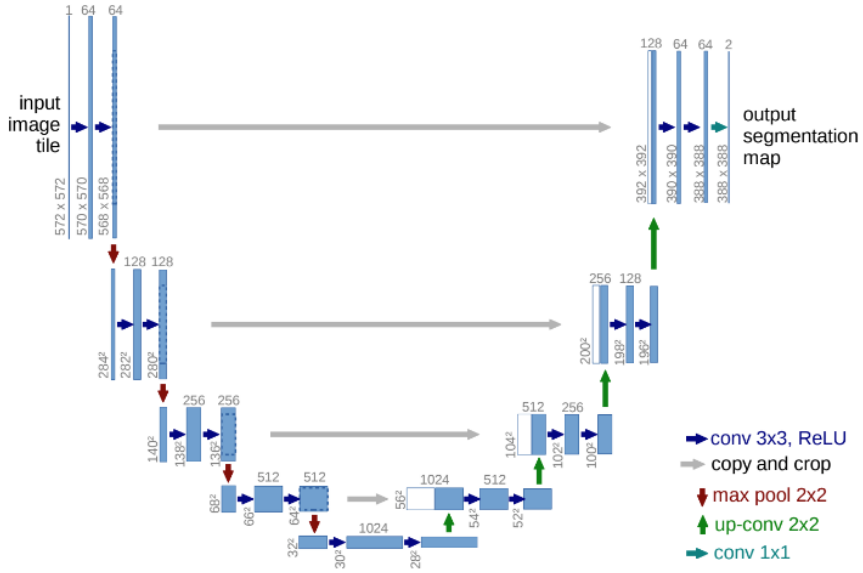

Figure 22 - U-Net Architecture

2.4 Data and Processing

For this project there were three main sources of data considered: Sentinel-1 imagery for the training of the network and application of the segmentation method; high resolution orthophotos to obtain a ground truth so that the outputs could be validated; and tide charts for the region to ensure that the tide heights observed in our images do not have a significant variation between them in order to avoid unnecessary errors in the results as the study area is quite flat.

Figure 3 depicts the workflow followed during this process.

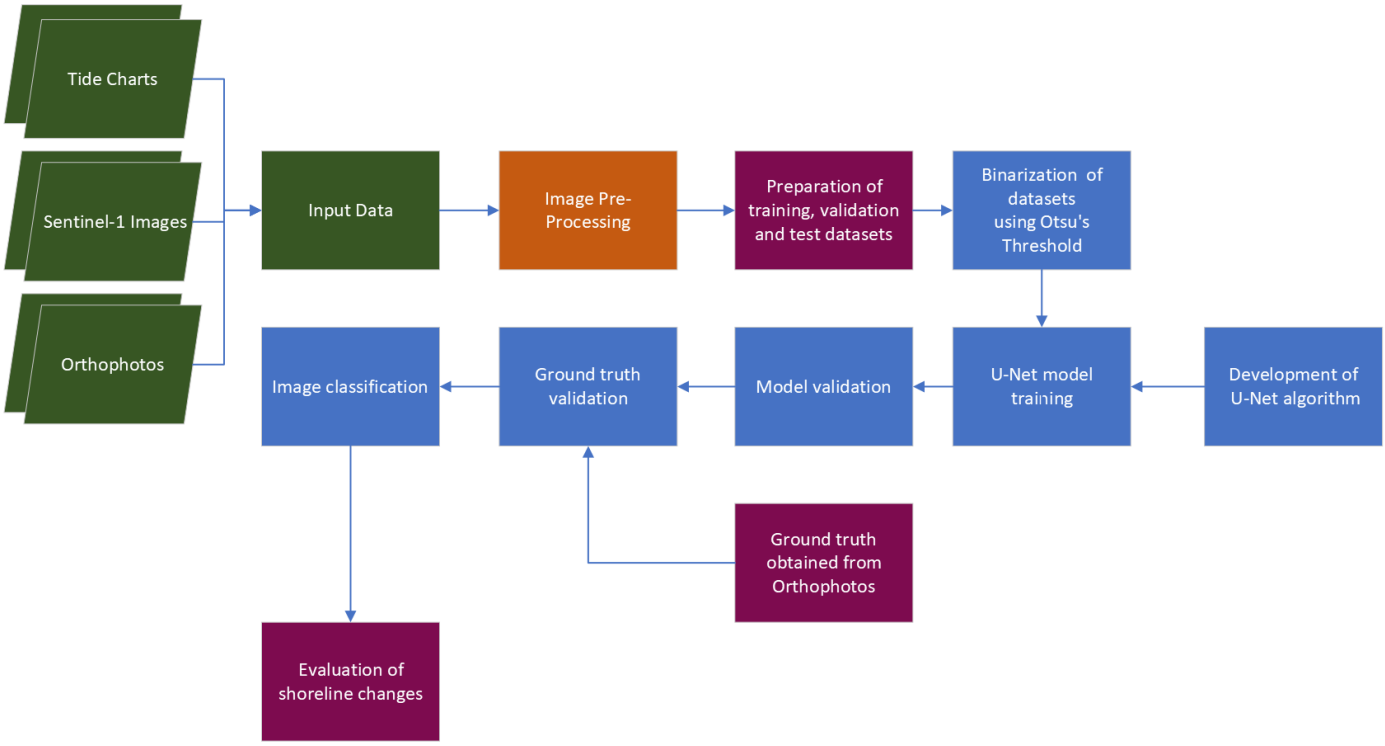

Figure 33 *- Project Workflow. Blue - Steps completed in Python, Orange - Steps completed in SNAP, Burgundy - Steps completed in QGIS, Green - Data aquisition from several sources*

The orthophotos used are open data provided by *Direção-Geral do Território* (DGT) and made publicly available as a WMTS service in SNIG (*"Sistema Nacional de Informação Geográfica"*) website [30]. The orthophotos in the region of interest were taken on the 15th of June 2018 between 14:45 and 15:30. Using the open-source software Q-GIS, an approximate ground truth line was digitised while using the highest possible resolution. An example of this can be seen in figure 4.

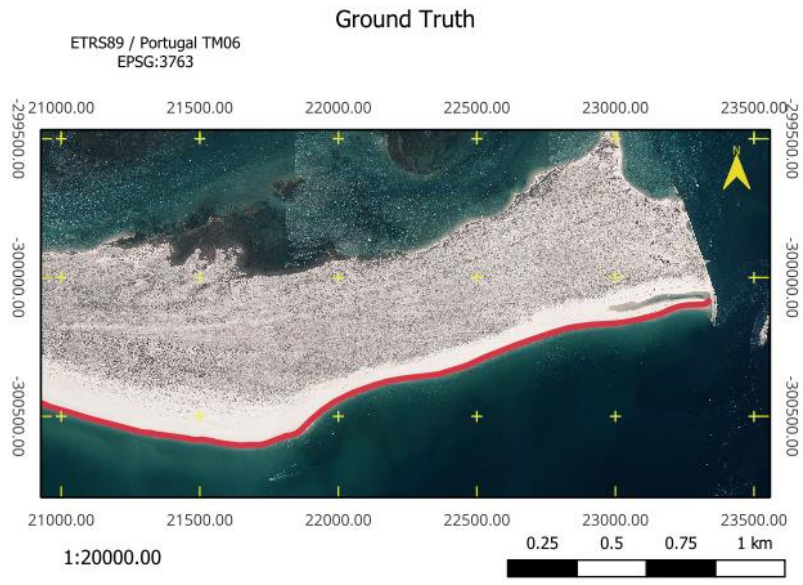

Figure 44 *- Ground Truth*

The tide charts were obtained from the website "*TabuaDeMares*"[31] for the tide gauge in nearby Faro and all satellite images were obtained considering the tide height at the time of image capture. A summary of the information can be seen in table 1.

The shoreline detection study was based on SAR data acquired by Sentinel-1, a constellation of earth observation satellites of the European Space Agency (ESA). Currently there is only one operational satellite (S1A) in the constellation, however some of the acquired images were taken by S1B which is currently inactive. The images for this project were open access and obtained from the Alaska Satellite Facility website [32]. In order to attempt to obtain satellite images as close to the orthophotos as possible, three images from June 2018 were downloaded. For the oldest image data, the closest tide height image available was from November 2014, so in order to account for any possible seasonal variations the most recent image obtained was from November 2022.

Table 1 *- Summary of input data*

Data Source	Date	Tide Height
Orthophotos	15/06/2018	3.2m
S1B_IW_GRDH_1SDV_ 20180619T183412_20180619T183437_011446_015069_8D92	19/06/2018	2.8m
S1B_IW_GRDH_1SDV_ 20180614T182602_20180614T182627_011373_014E30_CF2A(1)	14/06/2018	2.8m
S1A_IW_GRDH_1SDV_ 20180614T063517_20180614T063542_022349_026B6F_C513	14/06/2018	2.2m
S1A_IW_GRDH_1SDV_ 20141125T183433_20141125T183458_003442_00405B_E693(2)	25/11/2014	2.9m
S1A_IW_GRDH_1SDV_ 20221126T182654_20221126T182719_046069_058398_8AE6(3)	26/11/2022	2.7m

For the final validation process image (1) was chosen, while images (2) and (3) will be used to attempt to calculate a temporal variation of the coastline.

Following acquisition all satellite images were pre-processed in SNAP using the workflow proposed by Filliponi [33], seen in figure 5, followed by a subset of the region of interest in images (1), (2) and (3) and a subset of the coastal areas on all images. Finally, before exporting all the resulting images as GEOTIFF files a band subset was performed, keeping only the VV band as it performs better in this type of classification[34].

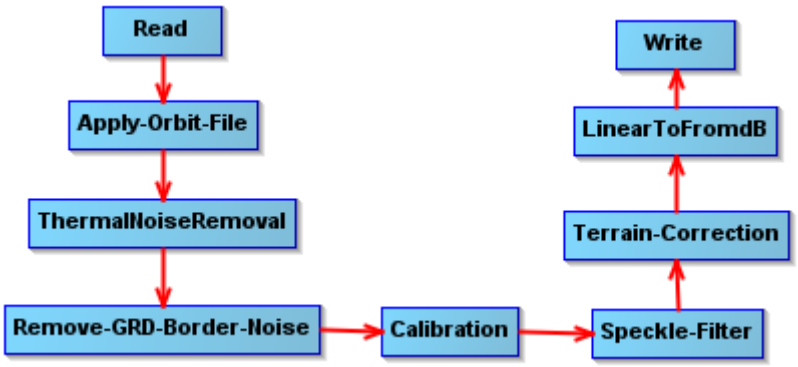

Figure 55 *- Pre-processing workflow*

2.5 Methodology

In order to prepare the training set to be used in the U-Net algorithm, first the images resulting from the pre-processing were imported in Q-GIS and divided into tiles measuring 256 x 256 pixels. This is due to the fact that deep learning algorithms usually work only with reduced size images for processing reasons and the authors of the article chose these dimensions. Following this the tiles were visually inspected to ensure they contained a coastline area. Due to the previously discussed limitations of the segmentation with Otsu's threshold which will be used to generate the masks, any tile where the land or sea area is very small cannot be used for training the network and therefore must be discarded in this phase. All coastal areas not included in the region of interest will be used for the training set.

Following this step, the images are imported into Python where they are first subjected to a data augmentation step, which consists in an artificial inflation of the original dataset, usually created by applying simple transformations which allow for the addition of more examples at with low workload. The main dangers of this method are the overfitting of the model if the data is concentrated on areas with very specific features[35], however in this case the large extension of the training images, as well as the variation in the types of coast landform serves as a counterbalance to try and prevent this problem from occurring. An example of the processing done to the tiles can be seen in figure 6.

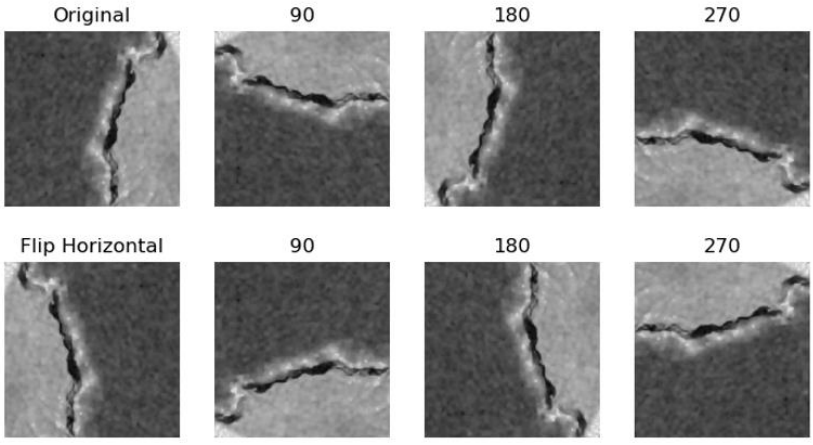

Figure 6 *- Data Augumentation step, with original figure (top left) being rotated and flipped*

To each original image a rotation of 90, 180 and 270 degrees was applied, followed by a left to right flip of the original image and a repetition of the three rotations. Once this step was completed a normalization of the image names was perform in order to more easily match the training labels with the images.

The training labels were also generated with Python, using morphology processing, namely the Otsu thresholding method. Just as the authors, a process of progressive smoothing of the original result obtained was followed through a series of dilations and erosions. The main issue here is due to the large dataset the structuring elements used for erosions and dilations can work well for some images but not for others – smaller elements may not be enough to remove noise from certain images but larger elements may misidentify land areas as water especially in zones with complex canal systems as is the case in Ria Formosa. An example of this processing can be seen in figure 7.

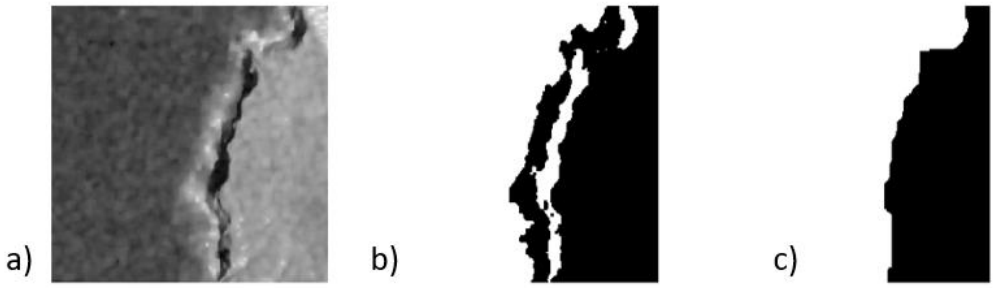

Figure 7 *- Example of Otsu's Thresholding - a) original tile, b) application of Otsu's threshold, c) smoothing with morphology operations*

Unlike the authors, most of the issues encountered in the training areas were on rocky coastal landforms due to a high brightness area immediately next to the shoreline, possibly due to the waves crashing into the cliffs and higher amounts of sand being in those areas, as seen in figure 8.

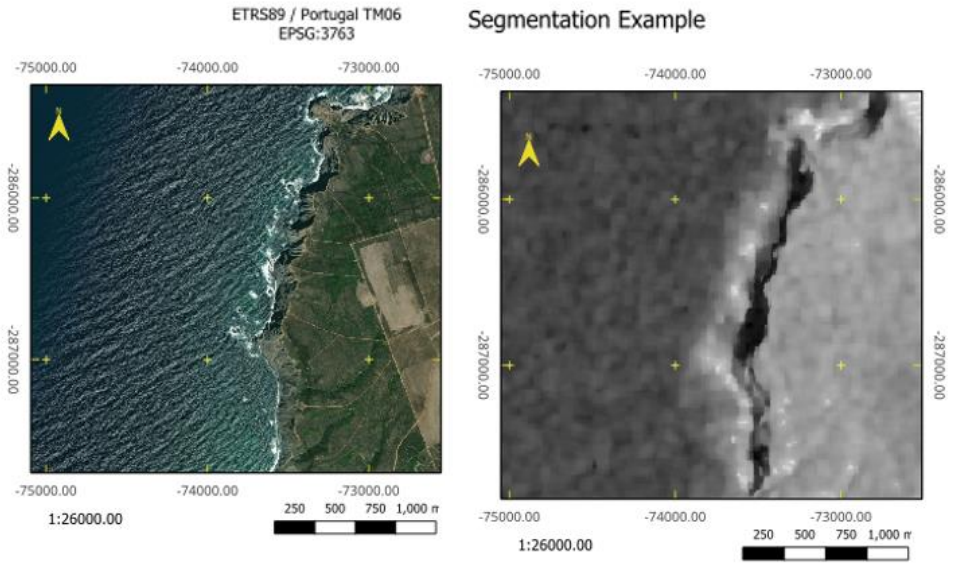

Figure 8 *- Landforms for segmentation example*

After this process was completed, another visual check was performed on the training label data to ensure that all the tiles had a clear land and sea distinction. Images where the training labels were not clear were also discarded.

The resulting training dataset contains 2664 images. From this dataset, 266 images (10%) were chosen using a random number selector to generate the U-Net results evaluation (confusion matrix). The leftover 2398 images are then further split inside the U-Net algorithm into a training set (80% - 1918 images) and a validation set (20% - 480 images) for internal validation and improvement of the model.

The U-Net algorithm itself was created based on open-source code available on GitHub both for a simple U-Net framework [36] and a deeper U-Net framework [37]. It starts by importing the training dataset and applying a median filter to remove noise followed by a normalization (division by 255) of the result. The dataset is then split as described previously. The network part of the code is composed by a five-step contracting path, where each step is composed of two stacks of 3x3 convolution, normalization, and activation, followed by a max pooling layer. Once the end of the contracting path is reached, it then starts a four-step expanding path, where each step is composed by one stack of 2x2 convolution, normalization and activation and two stacks of 3x3 convolution, normalization and activation layers. A more detailed version of the model used is available for download in the supplementary materials section.

The model is then trained with the training data and fitted to the validation data. For this process a batch size of 6 was chosen due to computational limitations, as the authors of the original article used a batch size of 16. The batch size is mostly limited by the GPU/CPU memory available, and it was chosen based on a process of trial and error. The model was trained and fitted over 100 epochs, with a "patience" condition where if the model would not improve for 5 epochs in a row the learn rate would be progressively lowered, until it reached a defined value, after which the next time the model would not improve for 10 epochs in a row the fitting would come to an early stop and save the weights of the best model. During this training process, the U-Net validates itself, internally generating masks for the training and validation datasets so it can evaluate its accuracy and loss.

The next step in the code is to visualise the result obtained by using one of the images and its mask, as seen in figure 9, and attempting to find an optimal threshold for the binarization of the result. From the learning experience gained in this process, this threshold is usually the approximately the validation accuracy obtained by the U-Net's evaluation step. This threshold is only necessary due to the size of the training dataset, as a larger input could give the algorithm more certainty when classifying pixels. Once this threshold is determined, the final step is to apply the model to our test set and extract the binary masks. These masks calculated by the U-Net are then compared with the original masks created with Otsu's Threshold, and a confusion matrix is generated.

Lastly, the model is applied to the region of interest. The resulting tiles are then georeferenced and joined together into the dimensions of the original image. Following a process of canny edge detection, which in the case of binary images can be simplified

into a subtraction of the eroded image from the original image, the shoreline is obtained from the classified image with Python, as shown in figure 10.

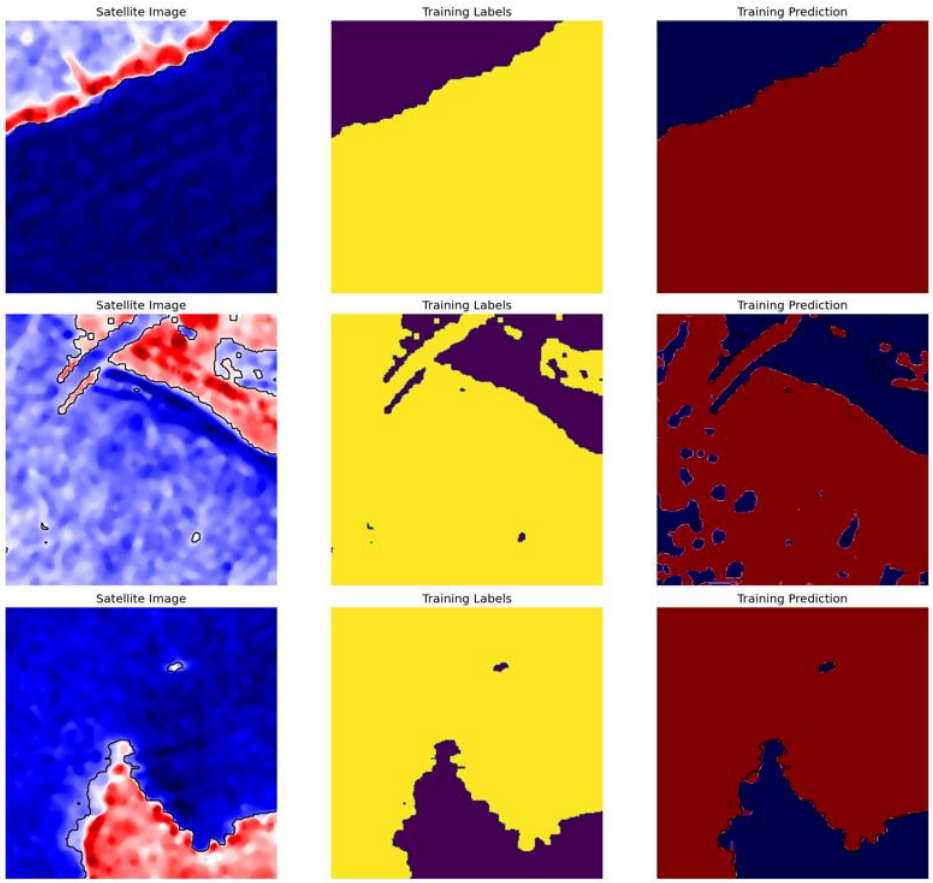

Figure 9 *- U-Net labels vs predictions*

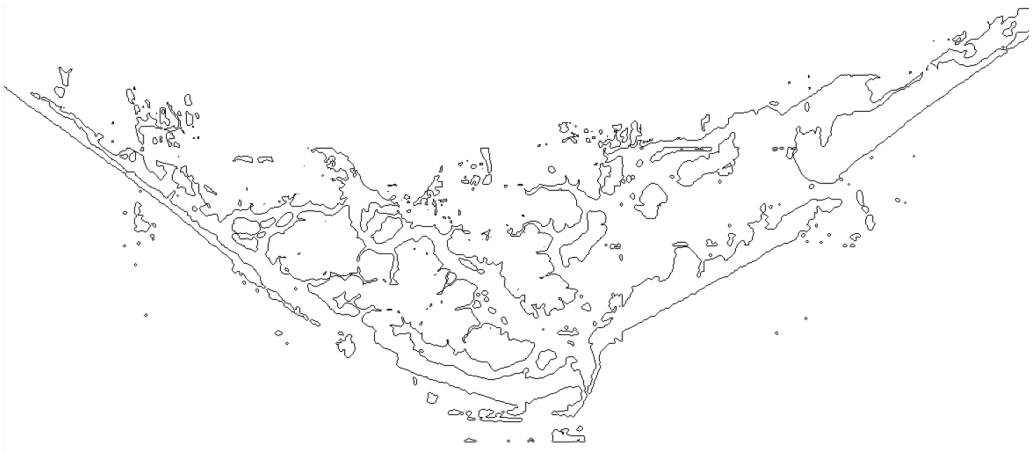

Figure 10 *- Shoreline extracted from edge algorithm*

Due to the existence of noise in certain regions of the classified image, the coast of the north-eastern barrier island was chosen to validate the classification. The obtained shoreline was once again georeferenced and vectorised in QGIS so that just the ocean shoreline could be extracted from the image. This was then converted into a raster file to be validated against the ground truth obtained from the orthophotos. An example of the difference between shorelines can be seen in figure 11.

Figure 11 *- Shoreline Difference*

3. Results

The main component of this project was the creation and training of the U-Net algorithm. As previously discussed, the model was trained with approximately 70% training images, 20% verification images and 10% testing images. The training process lasted approximately 57 hours and came to an early stop after 63 epochs. The training progress of the U-Net model can be seen in figures 12 and 13 and the best model results in table 2. The accuracy and loss of the best model for the training set were 96.1% and 0.117, respectively, while for the validation set it achieved 94.9% and 0.144, respectively.

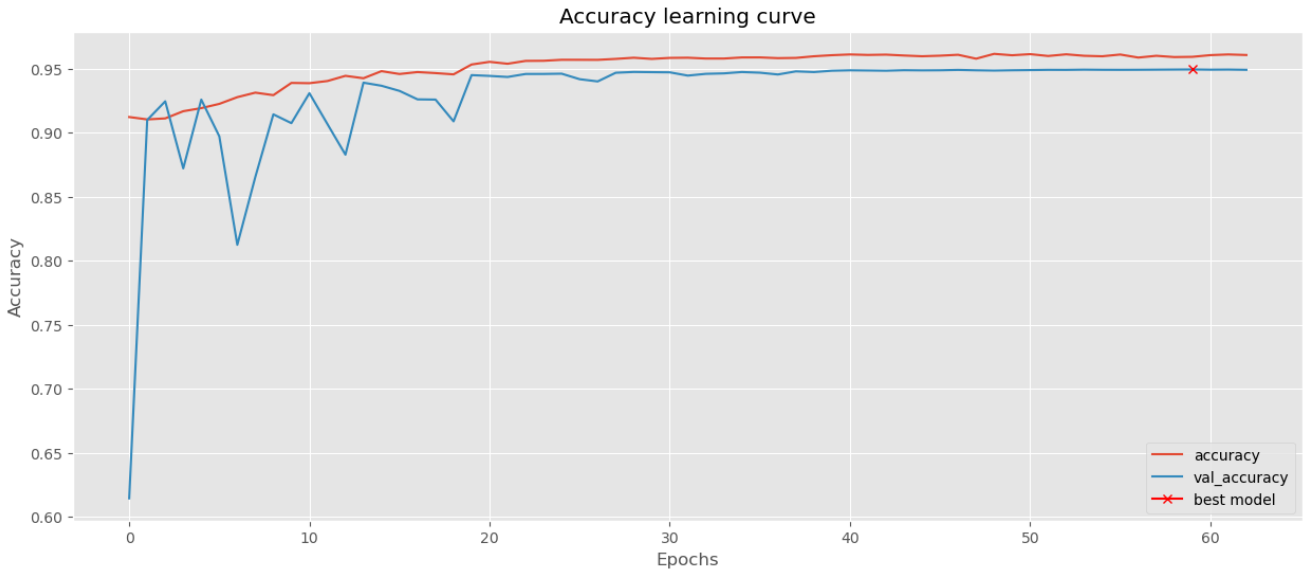

Figure 12 *- Accuracy learning curve*

Figure 13 - Loss learning curve

Table 2 - U-Net best model results

epoch	loss	accuracy	validation loss	validation accuracy
52	0.117	0.961	0.144	0.949

Following the U-Net's self-evaluation of the training, the randomly generated test data set was classified using the weights model of the output, and training labels were also generated for it using the Otsu's threshold method. Following this, a confusion matrix was compiled, which compares the result of the classification conducted by the algorithm with the threshold generated labels. For this confusion matrix the metrics used are precision, the proportion of true positives in the universe of all positives detected in the model, and the recall, the proportion of true positives in the universe of all the positives that should have been identified. Finally, there is also a need to calculate the overall accuracy (OA), following equation 2, the percentage of pixels which have been correctly classified (CC) in the total sample (TS).

$$overall\ accuracy = \frac{CC}{TS} \quad (2)$$

Other metrics that were calculated were the K-Coefficient, described in equation 3 and which consists of a measure of general statistical concordance of the matrix, taking into account all the classification and not only the correctly classified pixels, and the F1 Score, shown in equation 4, which is the weighted average between precision and recall. Unlike the other metrics, the F1 score is determined for all classes individually.

$$K = \frac{N\sum_{i=1}^{n} m_{i,i} - \sum_{i=1}^{n} G_i C_i}{N^2 - \sum_{i=1}^{n} G_i C_i} \quad (3)$$

$$F1\ score = 2 \times \frac{precision \times recall}{precision + recall} \quad (4)$$

The test dataset reached an overall accuracy of 81%, with Kappa Coefficient of 62% and F1 Score of both classes approximately 80%, as shown in table 3:

Table 3 *- Confusion Matrix of the Test Dataset*

		PREDICTED				
		0	1	Sum Rows	Recall	F1 Score
REAL	0	6681526	78541	6760067	0.988	0.799
	1	3284405	7388104	10672509	0.692	0.815
	Sum Col	9965931	7466645	17432576		
	Precision	0.670	0.989			
	OA	0.807				
	KappaC	0.626				

For the evaluation of the shoreline detection, the classification resulting from the U-Net model followed a process of binary morphology to transform from a segmentation of land-sea to the boundary line that divides the two. The ground truth which had been created previously was converted from a vector into a raster image and a confusion matrix was calculated, however, in this case, the only metrics of interest are the precision and F1 Score of the class representing the shoreline, as the only interest here is understanding how much of it was correctly classified. The distance to the ground truth is then increased by one pixel on each iteration, and the process repeated in order to understand how far from the ground truth is the result obtained from the U-Net classification. The results of this process can be seen in table 4.

Table 4 *- Confusion Matrix results for the shoreline detection within n pixels from the ground truth*

	0 px	1 px	2 px	3 px	4 px	5 px
Precision	0.004	0.094	0.246	0.413	0.559	0.742
F1 Score	0.004	0.091	0.220	0.344	0.439	0.543

While the authors of the original article reached over 90% F1 Score within 5 pixels, the model presented here was only able to reach 54.3% in this metric within 5 pixels. The totality of the shoreline was found to be within 10 pixels of the ground truth, which translates to approximately 100 m on the ground, considering the pixel size of Satellite-1 images.

With regards to shoreline changes, the image from 2022 unfortunately had a very poor classification with the algorithm, possibly due to a higher than usual amount of noise present in the image, as seen on figure 14 below. For this reason, only the shorelines from 2014 and 2018 were compared, as shown in figure 15, where there is a clear difference between the two lines. However, as shown above, the method used did not reach the high levels of accuracy that the model proposed by the authors reached, which means that the difference could simply be explained by the lower accuracy of the model, or the fact that the images correspond to different seasons of the year which means the difference could also be explained by natural phenomena such as the seasonal difference in sedimentation rates [38] or human activity such as beach nourishment plans [39]

***Figure 14**- Poor classification result obtained for 2022*

***Figure 15** - Shoreline difference between 2014 and 2018*

The difference in area between these two shorelines comes to a total of 62 963 m², which seems like a large number for a region that measures approximately 6 km across in such a short period of time, therefore this method would still need to be further improved before it could be applied to the monitoring of shoreline changes and it would need to be combined with more studies to validate the results in the region.

4. Discussion

Following the implementation of this project, the results obtained fell short of the expectations set by the original work.

The U-Net was developed for academic purposes and as such had to use a much smaller image sample size due to time constraints and therefore was unable to reach such high accuracy and low loss values as the one implemented by the authors, with the original U-Net reaching an accuracy of 99.5% with a loss of 0.005 and validation set accuracy

of 99.2% and loss of 0.019, while this U-Net was only able to reach an accuracy of 96.1% and loss of 0.117 and validation set accuracy of 94.9% and loss of 0.144. This necessitated the addition of an extra processing step in the code, where a threshold was defined based on the accuracy of the U-Net prediction, as it was not confident enough in its classification to return a binary image. An example of a pre-threshold output from the U-Net classification can be seen in figure 16.

Figure 16 *- U-Net output prior to threshold*

The results obtained were then georeferenced and converted into a shoreline, which was then compared to the ground truth shoreline visually obtained with high resolution orthophotos, however, possibly due to the less accurate U-Net and subjective nature of the ground truth digitalization, the results were once again less accurate than those obtained by the authors – in the original article an F1 Score of over 90% was reached within 5 pixels of the ground truth shoreline, while in this case the F1 score was only able to reach 54% within the same distance threshold.

These results greatly limit the application of this data to shoreline change monitoring as they are not able to reach the precision necessary to detect slight changes between epochs.

This work could be improved by the introduction of a larger image training sample, both in terms of number of images and temporal distribution. The method that is being used to generate the training labels, Otsu's Threshold, is also limited as it is not able to correctly separate images where one class has an area much smaller than the other and it also required smoothing of the labels after these are generated, which means the quality of the results can also be compromised if the images and masks which are input into the model are not visually inspected beforehand. This implies an extra layer of work which could be very daunting for larger image datasets. There are other segmentation methods which could potentially be used for the training labels – a method like hysteresis threshold could potentially solve issues such as sand banks that form just below the surface and that interfere in with the shoreline detection.

In this project, the only shoreline evaluated was a sandy landform, however the training dataset included images of other types of coast landform. It could be interesting to understand if the model would fare better at classifying the targeted area with a more targeted training dataset, however this was not the objective of the authors. There is also the possibility that the U-Net in this project would achieve better results classifying a

rocky shore, as they have features which are generally easier to separate, and those results would match the results the authors achieved in the original work.

During the research conducted for this project, other U-Net implementations were also researched, which could also potentially improve the results obtained, in particular, the Deep U-Net.

Following all the results obtained and their analysis it can be concluded that the approach used was adequate however it would need to be greatly expanded in order to be applied to the desired scale of coastline monitoring.

5. Conclusions

The objective of this project was to use a U-Net algorithm to automatically extract a land-sea classification from Sentinel-1 images, from which an automatic shoreline detection model could be constructed in order to monitor shoreline changes across periods of time.

The U-Net CNN was implemented successfully, however it failed to reach the high accuracy and low loss of the original work due to a much smaller training sample. Due to this, the classification of land-sea was not as successful, and the coastline detection was only able to reach an F1 Score of 54% within 5 pixels of the ground truth.

Supplementary Materials: The python code used in this project can be downloaded at https://github.com/SilviaMourao/DRMicro. The image datasets and trained U-Net model can be downloaded at https://we.tl/t-YT3bKcoUew.

References

[1] Antunes, C.; Madeira, F. *Analysis of Sea-Level Rise*; 2017.

[2] Madeira, F.; Antunes, C. Análise Da Variabilidade Relativa Do Nível Do Mar Para a Região Do Algarve; 2017.

[3] Dieng, H. B.; Cazenave, A.; Meyssignac, B.; Ablain, M. New Estimate of the Current Rate of Sea Level Rise from a Sea Level Budget Approach. *Geophys Res Lett*, **2017**, *44* (8), 3744–3751. https://doi.org/10.1002/2017GL073308.

[4] Cazenave, A.; Dieng, H. B.; Meyssignac, B.; von Schuckmann, K.; Decharme, B.; Berthier, E. The Rate of Sea-Level Rise. *Nature Climate Change 2014 4:5*, **2014**, *4* (5), 358–361. https://doi.org/10.1038/nclimate2159.

[5] Chen, X.; Zhang, X.; Church, J. A.; Watson, C. S.; King, M. A.; Monselesan, D.; Legresy, B.; Harig, C. The Increasing Rate of Global Mean Sea-Level Rise during 1993–2014. *Nature Climate Change 2017 7:7*, **2017**, *7* (7), 492–495. https://doi.org/10.1038/nclimate3325.

[6] Mutaqin, B. W. Shoreline Changes Analysis in Kuwaru Coastal Area, Yogyakarta, Indonesia: An Application of the Digital Shoreline Analysis System (DSAS). *International Journal of Sustainable Development and Planning*, **2017**, *12* (7), 1203–1214. https://doi.org/10.2495/SDP-V12-N7-1203-1214.

[7] Chang, L.; Chen, Y. T.; Wu, M. C.; Alkhaleefah, M.; Chang, Y. L. U-Net for Taiwan Shoreline Detection from SAR Images. *Remote Sensing 2022, Vol. 14, Page 5135*, **2022**, *14* (20), 5135. https://doi.org/10.3390/RS14205135.

[8] Zhu, Z.; Woodcock, C. E.; Rogan, J.; Kellndorfer, J. Assessment of Spectral, Polarimetric, Temporal, and Spatial Dimensions for Urban and Peri-Urban Land Cover Classification Using Landsat and SAR Data. *Remote Sens Environ*, **2012**, *117*, 72–82. https://doi.org/10.1016/J.RSE.2011.07.020.

[9] Niu, X.; Ban, Y. Multi-Temporal RADARSAT-2 Polarimetric SAR Data for Urban Land-Cover Classification Using an Object-Based Support Vector Machine and a Rule-Based Approach. *http://dx.doi.org/10.1080/01431161.2012.700133*, **2012**, *34* (1), 1–26. https://doi.org/10.1080/01431161.2012.700133.

[10] Lee, J. sen; Jurkevich, I. Coastline Detection and Tracing in SAR Images. *IEEE Transactions on Geoscience and Remote Sensing*, **1990**, *28* (4), 662–668. https://doi.org/10.1109/TGRS.1990.572976.

[11] Horritt, M. S. A Statistical Active Contour Model for SAR Image Segmentation. *Image Vis Comput*, **1999**, *17* (3–4), 213–224. https://doi.org/10.1016/S0262-8856(98)00101-2.

[12] Mason, D. C.; Davenport, L. J. Accurate and Efficient Determination of the Shoreline in ERS-1 SAR Images. *IEEE Transactions on Geoscience and Remote Sensing*, **1996**, *34* (5), 1243–1253. https://doi.org/10.1109/36.536540.

[13] Tello Alonso, M.; Lopez-Martinez, C.; Mallorqui, J. J.; Salembier, P. Edge Enhancement Algorithm Based on the Wavelet Transform for Automatic Edge Detection in SAR Images. *IEEE Transactions on Geoscience and Remote Sensing*, **2011**, *49* (1 PART 1), 222–235. https://doi.org/10.1109/TGRS.2010.2052814.

[14] Liu, Z.; Li, F.; Li, N.; Wang, R.; Zhang, H. A Novel Region-Merging Approach for Coastline Extraction from Sentinel-1A IW Mode SAR Imagery. *IEEE Geoscience and Remote Sensing Letters*, **2016**, *13* (3), 324–328. https://doi.org/10.1109/LGRS.2015.2510745.

[15] Demir, N.; Kaynarca, M.; Oy, S. EXTRACTION OF COASTLINES WITH FUZZY APPROACH USING SENTINEL-1 SAR IMAGE. https://doi.org/10.5194/isprsarchives-XLI-B7-747-2016.

[16] Mazzolini, M.; Manzoni, M.; Monti-Guarnieri, A. v.; Petrushevsky, N. SAR-BASED COASTLINE DETECTION AND MONITORING. *INTERNATIONAL ARCHIVES OF THE PHOTOGRAMMETRY, REMOTE SENSING AND SPATIAL INFORMATION SCIENCES*, **2021**, *XLIII-B3-2021* (B3-2021), 327–334. https://doi.org/10.5194/ISPRS-ARCHIVES-XLIII-B3-2021-327-2021.

[17] Ronneberger, O.; Fischer, P.; Brox, T. U-Net: Convolutional Networks for Biomedical Image Segmentation. *Lecture Notes in Computer Science (including subseries Lecture Notes in Artificial Intelligence and Lecture Notes in Bioinformatics)*, **2015**, *9351*, 234–241. https://doi.org/10.1007/978-3-319-24574-4_28/COVER.

[18] Baumhoer, C. A.; Dietz, A. J.; Kneisel, C.; Kuenzer, C. Automated Extraction of Antarctic Glacier and Ice Shelf Fronts from Sentinel-1 Imagery Using Deep Learning. *Remote Sensing 2019, Vol. 11, Page 2529*, **2019**, *11* (21), 2529. https://doi.org/10.3390/RS11212529.

[19] Heidler, K.; Mou, L.; Baumhoer, C.; Dietz, A.; Zhu, X. X. HED-UNet: Combined Segmentation and Edge Detection for Monitoring the Antarctic Coastline. *IEEE Transactions on Geoscience and Remote Sensing*, **2022**, *60*. https://doi.org/10.1109/TGRS.2021.3064606.

[20] Li, R.; Liu, W.; Yang, L.; Sun, S.; Hu, W.; Zhang, F.; Li, W. DeepUNet: A Deep Fully Convolutional Network for Pixel-Level Sea-Land Segmentation. *IEEE J Sel Top Appl Earth Obs Remote Sens*, **2018**, *11* (11), 3954–3962. https://doi.org/10.1109/JSTARS.2018.2833382.

[21] Chu, Z.; Tian, T.; Feng, R.; Wang, L. Sea-Land Segmentation with Res-Unet and Fully Connected CRF. *International Geoscience and Remote Sensing Symposium (IGARSS)*, **2019**, *2019-January*, 3840–3843. https://doi.org/10.1109/IGARSS.2019.8900625.

[22] Shamsolmoali, P.; Zareapoor, M.; Wang, R.; Zhou, H.; Yang, J. A Novel Deep Structure U-Net for Sea-Land Segmentation in Remote Sensing Images. *IEEE J Sel Top Appl Earth Obs Remote Sens*, **2019**, *12* (9), 3219–3232. https://doi.org/10.1109/JSTARS.2019.2925841.

[23] Newton, A.; Mudge, S. M. Temperature and Salinity Regimes in a Shallow, Mesotidal Lagoon, the Ria Formosa, Portugal. *Estuar Coast Shelf Sci*, **2003**, *57* (1–2), 73–85. https://doi.org/10.1016/S0272-7714(02)00332-3.

[24] Dias, J. M.; Sousa, M. C.; Bertin, X.; Fortunato, A. B.; Oliveira, A. Numerical Modeling of the Impact of the Ancão Inlet Relocation (Ria Formosa, Portugal). *Environmental Modelling and Software*, **2009**, *24* (6), 711–725. https://doi.org/10.1016/j.envsoft.2008.10.017.

[25] Xu, X.; Xu, S.; Jin, L.; Song, E. Characteristic Analysis of Otsu Threshold and Its Applications. *Pattern Recognit Lett*, **2011**, *32* (7), 956–961. https://doi.org/10.1016/J.PATREC.2011.01.021.

[26] Sankur, B. Survey over Image Thresholding Techniques and Quantitative Performance Evaluation. *J Electron Imaging*, **2004**, *13* (1), 146. https://doi.org/10.1117/1.1631315.

[27] Otsu, N. A Threshold Selection Method from Gray-Level Histograms. *TRANSACTIONS ON SYSTEMS, MAN, AND CYBERNETICS*, **1979**.

[28] Soares, F. Aulas de Processamento Digital de Imagem. 2022.

[29] Huang, B.; Zhao, B.; Song, Y. Urban Land-Use Mapping Using a Deep Convolutional Neural Network with High Spatial Resolution Multispectral Remote Sensing Imagery. *Remote Sens Environ*, **2018**, *214*, 73–86. https://doi.org/10.1016/j.rse.2018.04.050.

[30] SNIG :: Ortofotos 25 cm - Portugal Continental - 2018 https://snig.dgterritorio.gov.pt/rndg/srv/api/records/daf5479d-29c8-4e0c-b7b8-0e1791891186/formatters/snig-view (accessed Dec 12, 2022).

[31] Tabela de marés 2023 de Faro para a pesca https://tabuademares.com/pt/faro/faro (accessed Dec 12, 2022).

[32] ASF Data Search https://search.asf.alaska.edu/#/ (accessed Dec 12, 2022).

[33] Filipponi, F. Sentinel-1 GRD Preprocessing Workflow. *Proceedings 2019, Vol. 18, Page 11*, **2019**, *18* (1), 11. https://doi.org/10.3390/ECRS-3-06201.

[34] López-Caloca, A. A.; Tapia-Silva, F. O.; Guadalupe Rivera; López-Caloca, A. A.; Tapia-Silva, F. O.; Guadalupe Rivera. Sentinel-1 Satellite Data as a Tool for Monitoring Inundation Areas near Urban Areas in the Mexican Tropical Wet. *Water Challenges of an Urbanizing World*, **2017**. https://doi.org/10.5772/INTECHOPEN.71395.

[35] Taylor, L.; Nitschke, G. Improving Deep Learning Using Generic Data Augmentation. **2017**.

[36] Patel, A. satellite-Image-Semantic-Segmentation-Unet-Tensorflow-keras https://github.com/ashishpatel26/satellite-Image-Semantic-Segmentation-Unet-Tensorflow-keras/tree/main/Notebooks (accessed Dec 12, 2022).

[37] Kouyama, T. DeepUnet_Keras: Example of Keras implementation of Deep Unet https://github.com/TKouyama/DeepUnet_Keras (accessed Dec 12, 2022).

[38] Salmela, J.; Saarni, S.; Blåfield, L.; Katainen, M.; Kasvi, E.; Alho, P. Comparison of Cold Season Sedimentation Dynamics in the Non-Tidal Estuary of the Northern Baltic Sea. *Mar Geol*, **2022**, *443*, 106701. https://doi.org/10.1016/J.MARGEO.2021.106701.

[39] Staudt, F.; Gijsman, R.; Ganal, C.; Mielck, F.; Wolbring, J.; Hass, & H. C.; Goseberg, N.; Schüttrumpf, H.; Schlurmann, T.; Schimmels, S. The Sustainability of Beach Nourishments: A Review of Nourishment and Environmental Monitoring Practice. https://doi.org/10.1007/s11852-021-00801-y.